

4 The Kondo Model and Poor Man's Scaling

Andriy H. Nevidomskyy

Dept. of Physics and Astronomy, Rice University

6100 Main Street, Houston, TX 77005, USA

Contents

1	The Kondo problem: Introduction	2
2	Concept of renormalization	5
3	Poor man's scaling for the Kondo model	5
3.1	T -matrix description of scattering processes	5
3.2	Renormalization of J_z	7
3.3	Renormalization of J_{\pm}	8
3.4	Renormalization group flow	9
3.5	Kondo temperature and breakdown of the perturbative scheme	11
4	Low-temperature properties of the Kondo model	12
4.1	Wilson's numerical renormalization	12
4.2	Ground state of the Kondo model	13
5	Multichannel Kondo problem	14
5.1	Phenomenology and scaling	14
5.2	Two-channel Kondo problem	17
6	Kondo model in the presence of Hund's coupling	19
6.1	Poor man's scaling with Hund's coupling	21
6.2	Experimental ramifications of Hund's coupling	25

The Kondo model has played a very important role in condensed matter physics. Experimentally motivated, it attracted a great deal of theoretical attention in the 1960s and 1970s, resulting in the conclusion that thermodynamic and transport properties depended logarithmically on temperature as $\ln(T/T_K)$, where T_K is called the Kondo temperature. The ideas of summing up the leading logarithmic divergences and establishing how this procedure depended on the high-energy cutoff were instrumental in the development of the scaling theory and the renormalization group, which were initially invented in the 1950s in high-energy physics. Despite this progress, what was very puzzling was that the resulting theoretical predictions for the thermodynamic and transport properties displayed a divergence at $T \approx T_K$, at which point the theory became unusable. Was this logarithmic divergence physical and what was the fate of the model at low temperatures $T \ll T_K$? These questions remained unanswered for almost a decade, until the breakthrough made by Kenneth Wilson in 1974, who invented a numerical algorithm of renormalization, now known as the numerical renormalization group, and showed it to be stable down to very low temperatures [1]. Wilson's work was hugely influential, for which he was awarded the Nobel prize in physics in 1982. At the same time, Nozières had developed a phenomenological low-energy theory of the Kondo model [2], showing it to be a Fermi liquid, in agreement with Wilson's numerical conclusions. This was a triumph of theory, further corroborated when the exact solution of the Kondo model was found in 1980 [3, 4]. From a historical perspective, the Kondo model therefore clearly has an iconic status. However, this is not the only reason why this topic features prominently in several Lectures in this School. It can be said without exaggeration that the ideas of scaling and renormalization group developed *en route* to solving the Kondo problem represent a cornerstone in our current understanding of correlated many-body systems, applicable to both condensed matter and high-energy physics. In this Lecture, I will first briefly introduce the Kondo model, before discussing in detail the elegant renormalization argument invented by P.W. Anderson, the so-called Poor Man's scaling theory [5]. I will then summarize briefly Wilson's numerical renormalization group idea as well as the aforementioned Fermi liquid theory by Nozières. The discussion in these sections is loosely based on the original article by Anderson [5] as well as on the textbooks by Yamada [6] and Hewson [7]. Having thus introduced the concept of scaling and renormalization, I will further illustrate their value by applying these methods to the more complicated incarnations of the Kondo model based on the so-called multichannel Kondo model in Section 5 and Section 6. This lecture is self-contained; however it presumes that the reader is well versed in the language of second quantization and has some familiarity with Feynman diagrams. Other than this, no special prerequisites are necessary.

1 The Kondo problem: Introduction

It was noticed as early as the 1930s that the resistance of noble metals like gold or silver exhibits a minimum as a function of temperature, see Fig. 1. It was later realized that this effect arises from magnetic impurities such as Mn and Fe, which are naturally present in noble metals. In ordinary metals, the electrical resistance originates from the lattice umklapp scattering and

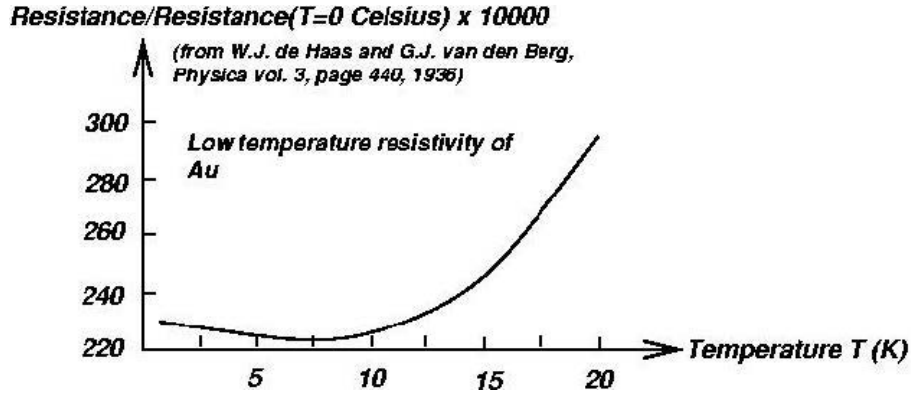


Fig. 1: Normalized resistance of Au with magnetic impurities as a function of temperature. (Reproduced from Ref. [8])

scattering off of impurities as well as lattice vibrations (phonons). When the temperature is lowered from room temperature, the resistance due to phonons decreases proportionally to T^5 . At much lower temperatures, when lattice vibrations are frozen out, the temperature dependence of resistance stems from the electron-electron interaction, which in ordinary metals scales as T^2 , consistent with the prediction of Landau's Fermi liquid theory. In any event, the resistance of a regular metal is a monotonically decreasing function as the temperature is lowered. By contrast, in dilute magnetic alloys the resistance starts increasing again with decreasing temperature.

This behavior of the resistance remained a puzzle until 1964, 30 years after the experimental discovery, when Jun Kondo presented the theory that explains the resistance minimum [9]. Kondo wrote down the model in which the dilute magnetic impurities are described by spin variables $\mathbf{S}(\mathbf{R}_i)$ at positions \mathbf{R}_i that interact with conduction electrons via a spin-spin interaction. Since the impurities are randomly distributed and dilute, it is sufficient to consider one such impurity interacting with conduction electrons:

$$H = \sum_{\mathbf{k}, \sigma} \varepsilon_{\mathbf{k}} c_{\mathbf{k}\sigma}^\dagger c_{\mathbf{k}\sigma} + 2J \mathbf{s} \cdot \mathbf{S}, \quad (1)$$

where conduction electron spin \mathbf{s} at the impurity site $\mathbf{R} = 0$ is defined as $\mathbf{s}(\mathbf{R}) = \frac{1}{2} c^\dagger(\mathbf{R}) \boldsymbol{\sigma} c(\mathbf{R})$ (setting $\hbar = 1$ for convenience). The spin interaction in the last term arises from the exchange interaction between a conduction electron (for instance, in an s -shell of Au) and the localized electron (d -shell in the case of transition metal impurities). The above model is often referred to as the s - d model or, equivalently, as the Kondo model (in what follows, we shall adopt the latter nomenclature). The factor of 2 in front of the interaction is chosen for convenience.

Equivalently, the model can be re-written by Fourier transforming the conduction electron creation/annihilation operators to the reciprocal space as follows:

$$H = \sum_{\mathbf{k}, \sigma} \varepsilon_{\mathbf{k}} c_{\mathbf{k}\sigma}^\dagger c_{\mathbf{k}\sigma} + J \sum_{\mathbf{k}, \mathbf{k}'} c_{\mathbf{k}'\sigma'}^\dagger \boldsymbol{\sigma}_{\sigma'\sigma} c_{\mathbf{k}\sigma} \cdot \mathbf{S}, \quad (2)$$

with the summation over spin indices σ, σ' implied. One can further generalize this model by allowing anisotropy of the exchange interaction:

$$H = \sum_{\mathbf{k}, \sigma} \varepsilon_{\mathbf{k}} c_{\mathbf{k}\sigma}^\dagger c_{\mathbf{k}\sigma} + J_z \sum_{\mathbf{k}, \mathbf{k}'} \sum_{\sigma} c_{\mathbf{k}'\sigma}^\dagger \sigma_{\sigma\sigma}^z c_{\mathbf{k}\sigma} \cdot S_z + \frac{1}{2} \sum_{\mathbf{k}, \mathbf{k}'} \left(J_- c_{\mathbf{k}'\uparrow}^\dagger c_{\mathbf{k}\downarrow} S^- + J_+ c_{\mathbf{k}'\downarrow}^\dagger c_{\mathbf{k}\uparrow} S^+ \right), \quad (3)$$

where as usual $S^\pm \equiv S_x \pm iS_y$. In what follows, we shall assume the transverse spin interaction to be isotropic: $J_+ = J_- = J_\pm$ (in which case $J_\pm = J_x = J_y$ also follows).

In order to calculate the resistance of the model in Eq. (2), Kondo computed the scattering probability for conduction electrons using the T -matrix formalism [9, 10]. This formalism will be introduced in detail when discussing the scaling of the Kondo model in Section 3, so in order to avoid an unnecessary repetition, we shall only quote the final result for the resistance obtained by Kondo in the first Born approximation (see Ch. 4 of the book by Yamada [6] for more details):

$$R = R_0 \left[1 - 4J\rho \ln \left(\frac{k_B T}{D} \right) + \dots \right], \quad (4)$$

where R_0 is the residual (temperature-independent) resistance, D is the conduction electron bandwidth and ρ is the density of states at the Fermi level. As temperature decreases, $k_B T \ll D$ and the logarithm is negative, leading to a logarithmic increase of the resistance (and eventual divergence as $T \rightarrow 0$) provided $J > 0$. This is the essence of the Kondo effect, which explains the low-temperature behavior of the resistance in Fig. 1. At high temperatures, on the other hand, the aforementioned T^5 contribution to resistance from phonon scattering dominates, so that the resistance has a non-monotonic behavior with a minimum roughly around $T \sim T_K$.

We note that while historically, the position of the resistance minimum was often taken as a definition of the Kondo temperature, this is unsatisfactory because this definition depends on the details of the phonon scattering and the prefactor R_0 in Eq. (4). Instead, the modern approach is to define the Kondo temperature independently of the resistance. To see how one might go about this, consider the higher scattering processes (beyond the first Born approximation), which are implicitly contained in the “...” in Eq. (4). In fact, Abrikosov showed [11] that these terms yield an even stronger divergence as $T \rightarrow 0$ because they scale as $[J\rho \log(k_B T/D)]^n$. Summing the most divergent terms, Abrikosov obtained the result for resistance [11]

$$R = \frac{R_0}{\left[1 + 2J\rho \ln \left(\frac{k_B T}{D} \right) \right]^2}. \quad (5)$$

The Kondo temperature may be defined as the characteristic temperature at which the resistance diverges, which results in the estimate

$$k_B T_K \sim D \exp \left(-\frac{1}{2J\rho} \right). \quad (6)$$

As mentioned earlier in the introduction, other physical quantities, such as the magnetic susceptibility, were also shown to diverge logarithmically as the temperature $T = T_K$. Clearly, the theory cannot be trusted for low temperatures $T \lesssim T_K$, and this became the stumbling block of the Kondo problem until Wilson’s numerical solution in 1974 [1]. To understand how Wilson’s solution works, we have to first introduce the concept of renormalization and study how it applies to the Kondo model, which will be dealt with in the next two sections.

We note parenthetically that the divergence in Eq. (5) only occurs for the antiferromagnetic sign of the Kondo interaction ($J > 0$); otherwise, the resistance becomes small and converges. We shall explain the physical reason behind this behavior when we study the scaling of the Kondo model in Section 3.

2 Concept of renormalization

Usually, physical phenomena take place on a wide energy scale in condensed matter systems, from the conduction electron bandwidth of the order of several electron-volts, down to the experimentally relevant temperature range of the order of 1 Kelvin ($1 \text{ K} \approx 10^{-4} \text{ eV}$). We are interested in the low-energy (also called infra-red) limit, and the question is how to arrive there starting from the model formulated at high energy scales. The crucial idea is that instead of focusing on the fine details of the high-energy model (such as the exact spatial dependence of the interactions), one can arrive at the low-energy properties by monitoring the behavior of the system as one slowly lowers the cutoff scale Λ , which has the meaning of the energy corresponding to the largest-energy excitations available. If the system has a well-defined low-energy limit, the low-energy excitations will remain immune to this renormalization of the cutoff, and the model will be described by the “fixed point” Hamiltonian. In this case, the entire continuous family of model Hamiltonians $H(\Lambda)$ is said to “flow to the fixed point” and they belong to the same *universality class*. The word “universality” here implies that the low-energy behavior is universal, in other words, independent of the details of the high-energy (ultra-violet) model.

This idea of elucidating the low-energy universal behavior is achieved by the so-called *renormalization group* procedure, which consists of two steps:

1. Rescale the energy cutoff $\Lambda \rightarrow \Lambda' = \Lambda/b$, where $b > 1$, and integrate out the degrees of freedom in the energy range $[\Lambda/b, \Lambda]$. This will result in the change of the Hamiltonian $H(\Lambda) \rightarrow H'$.
2. Rescale the energy scales back so that $\omega = b\omega'$ and the new Hamiltonian $H(\Lambda/b) = bH'$.

These two steps are then repeated successively and in the limit $b \rightarrow 1$, one will obtain a continuous evolution of the model Hamiltonian with Λ . Below, we shall apply this idea to the Kondo model following P.W. Anderson's “Poor Man's scaling” argument [5].

3 Poor man's scaling for the Kondo model

3.1 T -matrix description of scattering processes

Following the general renormalization group ideas outlined above, we progressively integrate out the electronic states at the edge of the conduction band in the energy range $[\Lambda - \delta\Lambda, \Lambda]$. The resulting Hamiltonian will depend on the running energy scale Λ :

$$H(\Lambda) = \sum_{|\varepsilon_k| < \Lambda} \varepsilon_k c_{k\sigma}^\dagger c_{k\sigma} + J_z(\Lambda) \sum c_{k'\sigma'}^\dagger \sigma_{\sigma'\sigma}^z c_{k\sigma} \cdot S_z + \frac{J_\pm(\Lambda)}{2} \sum \left(c_{k'\uparrow}^\dagger c_{k\downarrow} S_- + c_{k'\downarrow}^\dagger c_{k\uparrow} S_+ \right), \quad (7)$$

where the last two terms correspond to the original Kondo Hamiltonian but with the renormalized coupling constant $J(\Lambda)$. This procedure was first performed by Anderson and Yuval using a

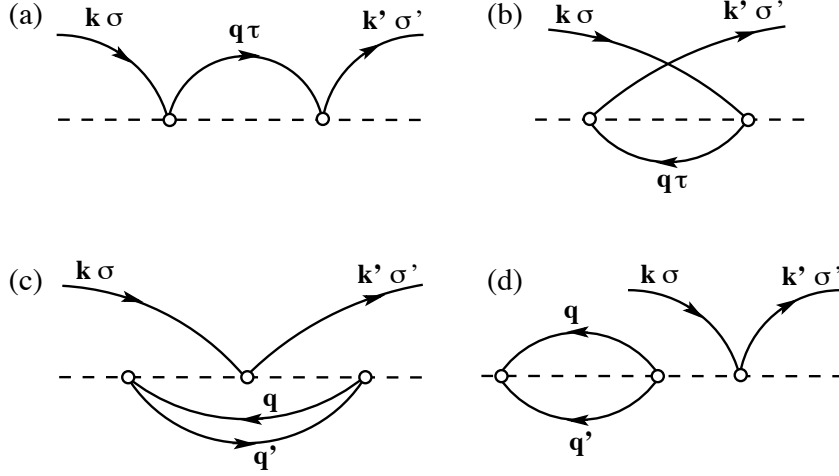


Fig. 2: Feynman diagrams contributing to (a,b) second-order processes in the Kondo interaction vertex (marked with an empty circle); and (c,d) third-order processes in the Kondo interaction. The solid lines denote the conduction electron propagator, whereas the dashed line denotes the impurity spin.

somewhat different method for a one-dimensional model equivalent to the Kondo model [12,13] and later reformulated by Anderson in a simplified form, which he called the “Poor Man’s” scaling approach [5]. The term “poor man” refers to the fact that the bandwidth is not rescaled to its original size after each progressive renormalization. This simplifies the matter as there is no need to rescale the Hamiltonian, eliminating the second step in the renormalization group procedure. Nevertheless, the results obtained via this simplified renormalization procedure are qualitatively accurate and correctly describe the low-energy behavior of the Kondo model.

Following Anderson, we integrate out the high-energy spin fluctuations using the formalism of the T -matrix, which describes the scattering of an electron from initial state $|\mathbf{k}\rangle$ into the final state $|\mathbf{k}'\rangle$. The matrix elements of such a scattering process constitute the so-called T -matrix, defined as a function of energy ω as follows:

$$T_{\mathbf{k}',\mathbf{k}}(\omega) = V_{\mathbf{k}',\mathbf{k}} + V_{\mathbf{k}',\mathbf{q}} G_0(\omega, \mathbf{q}) T_{\mathbf{q},\mathbf{k}}(\omega) = \hat{V} + \hat{V} \frac{1}{\omega - \hat{H}_0} \hat{T}(\omega), \quad (8)$$

where $H_0 = \sum_{k\sigma} \varepsilon_k c_{k\sigma}^\dagger c_{k\sigma}$ is the non-interacting conduction electron Hamiltonian, \hat{V} is the Kondo exchange interaction, and G_0 is the non-interacting Green’s function. In what follows, we shall calculate the T -matrix to second-order in the Kondo interaction $\hat{V} \propto J$, in which case we can replace $\hat{T} \rightarrow \hat{V}$ in the last term in Eq. (8). This corresponds to renormalizing the interaction $\hat{V} \rightarrow \hat{V}'$ with

$$\hat{V}' = \hat{V} + \hat{V} \frac{1}{\omega - \hat{H}_0} \hat{V} = \hat{V} + \Delta \hat{T}. \quad (9)$$

Two kinds of processes contribute to the T -matrix at this order: (a) the electron is scattered directly, as the Feynman diagram in Fig. 2a illustrates; or (b) a virtual electron-hole pair is created in the intermediate state, see Fig. 2b. In both cases, the intermediate state may occur with or without flipping the spin of the conduction electron/hole. Let us first consider the case

when the conduction electron spin is \uparrow both in the initial and in the final state. Consider first the simplest case when the conduction electron spin is not flipped in the intermediate state. The first process in Fig. 2a contributes

$$\Delta T_{\text{no-flip}}^{(a)}(\omega) = \sum_{\mathbf{q}}^{\Lambda > |\varepsilon_{\mathbf{q}}| > \Lambda - \delta\Lambda} (J_z)^2 S_z c_{\mathbf{k}'\uparrow}^\dagger c_{\mathbf{q}\uparrow} (\omega - \varepsilon_{\mathbf{q}} + \varepsilon_{\mathbf{k}} - \hat{H}_0)^{-1} S_z c_{\mathbf{q}\uparrow}^\dagger c_{\mathbf{k}\uparrow} \quad (10)$$

It is understood that T is a matrix depending on the external momenta and spin polarizations $\{\mathbf{k}' \uparrow, \mathbf{k} \uparrow\}$; however, we drop these indices for brevity. If the energy ω is measured relative to the Fermi level μ , then $\hat{H}_0 = \sum_{k\sigma} (\varepsilon_k - \mu) \hat{n}_k$ can be set to zero in the ground state. Since the summation over \mathbf{q} takes place in the narrow energy window $[\Lambda - \delta\Lambda, \Lambda]$, we can set $\varepsilon_{\mathbf{q}} \sim \Lambda$. Then, $c_{\mathbf{q}\tau} c_{\mathbf{q}\tau}^\dagger = 1 - \hat{n}_{\mathbf{q}}$ can be approximated as 1 in the particle-like intermediate state at low temperatures. Replacing the \mathbf{q} -summation with an integration over the density of states ρ , we thus obtain

$$\Delta T_{\text{no-flip}}^{(a)}(\omega) = \frac{(J_z)^2 |\rho \delta\Lambda| S_z S_z c_{\mathbf{k}'\uparrow}^\dagger c_{\mathbf{k}\uparrow}}{\omega - \Lambda + \varepsilon_{\mathbf{k}}} = \frac{(J_z)^2 |\rho \delta\Lambda|}{4(\omega - \Lambda + \varepsilon_{\mathbf{k}})} c_{\mathbf{k}'\uparrow}^\dagger c_{\mathbf{k}\uparrow}, \quad (11)$$

where we have used $S_z^2 = 1/4$ for a spin 1/2 impurity. This term does not depend on the impurity spin and contributes to the potential scattering only, resulting in an overall energy shift. The same conclusion is reached in the case of the second type of scattering given by Fig. 2b. Such potential scattering is a new term absent from the original Kondo model in Eq. (7); however, it is irrelevant in the renormalization group sense and does not qualitatively alter the behavior of the model.

3.2 Renormalization of J_z

Let us now consider the physically more interesting case where the conduction electron is scattered from a \uparrow to a \downarrow state with a spin-flip in the intermediate state. The first process in Fig. 2a yields the following contribution to the T -matrix:

$$\Delta T_{\uparrow\downarrow}^{(a)}(\omega) = \sum_{\mathbf{q}}^{\Lambda > |\varepsilon_{\mathbf{q}}| > \Lambda - \delta\Lambda} J_+ J_- S^- c_{\mathbf{k}'\uparrow}^\dagger c_{\mathbf{q}\downarrow} (\omega - \varepsilon_{\mathbf{q}} + \varepsilon_{\mathbf{k}} - \hat{H}_0)^{-1} S^+ c_{\mathbf{q}\downarrow}^\dagger c_{\mathbf{k}\uparrow}. \quad (12)$$

Similar to the earlier case, \hat{H}_0 can be set to zero in the ground state, and the intermediate state energy $\varepsilon_{\mathbf{q}} \sim \Lambda$. Given that $c_{\mathbf{q}\tau} c_{\mathbf{q}\tau}^\dagger = 1$ in the particle-like intermediate state at low temperatures, we thus obtain

$$\begin{aligned} \Delta T_{\uparrow\downarrow}^{(a)}(\omega) &= \sum_{\mathbf{q}}^{\Lambda - \delta\Lambda < \varepsilon_{\mathbf{q}} < \Lambda} J_+ J_- S^- S^+ c_{\mathbf{k}'\uparrow}^\dagger c_{\mathbf{k}\uparrow} (\omega - \varepsilon_{\mathbf{q}} + \varepsilon_{\mathbf{k}})^{-1} \\ &\approx J_+ J_- |\rho \delta\Lambda| S^- S^+ c_{\mathbf{k}'\uparrow}^\dagger c_{\mathbf{k}\uparrow} (\omega - \Lambda + \varepsilon_{\mathbf{k}})^{-1}. \end{aligned} \quad (13)$$

Similarly, the second process depicted in Fig. 2b yields

$$\begin{aligned} \Delta T_{\uparrow\uparrow}^{(b)}(\omega) &= \sum_{\mathbf{q}}^{-\Lambda < \varepsilon_{\mathbf{q}} < -\Lambda + \delta\Lambda} J_+ J_- S^+ c_{\mathbf{q}\tau}^\dagger c_{\mathbf{k}'\uparrow} (\omega + \varepsilon_{\mathbf{q}} - \varepsilon_{\mathbf{k}'})^{-1} S^- c_{\mathbf{k}\uparrow}^\dagger c_{\mathbf{q}\tau} \\ &\approx J_+ J_- |\rho \delta\Lambda| S^+ S^- c_{\mathbf{k}'\uparrow}^\dagger c_{\mathbf{k}\uparrow} (\omega - \Lambda - \varepsilon_{\mathbf{k}'})^{-1}, \end{aligned} \quad (14)$$

where we used the fact that in the hole-like intermediate state, the summation is near the lower band edge $[-\Lambda, -\Lambda + \delta\Lambda]$ and we can therefore replace $\varepsilon_q = -\Lambda$, with occupation number $c_{q\tau}^\dagger c_{q\tau} = 1$. We can now use the spin commutation relations on the impurity site to deduce that, for spin 1/2, $S^- S^+ = 1/2 - S_z$, and similarly $S^+ S^- = 1/2 + S_z$ (we have set $\hbar = 1$ for convenience). We conclude that the expressions in Eq. (13) and (14) contribute to the renormalization of the $J_z S_z c_{\mathbf{k}\uparrow}^\dagger c_{\mathbf{k}'\uparrow}$ term in the Kondo Hamiltonian. Similar expressions, but with the opposite sign, can be obtained starting from the conduction electron in the spin \downarrow state. We conclude that the J_z term in the Kondo interaction is renormalized as follows:

$$V'_z = (J_z + \delta J_z) \sum_{\mathbf{k}, \mathbf{k}'} \left(c_{\mathbf{k}\uparrow}^\dagger c_{\mathbf{k}'\uparrow} - c_{\mathbf{k}\downarrow}^\dagger c_{\mathbf{k}'\downarrow} \right) \cdot S_z, \quad (15)$$

with

$$\delta J_z = -J_+ J_- \rho |\delta\Lambda| \left[\frac{1}{\omega - \Lambda + \varepsilon_k} + \frac{1}{\omega - \Lambda - \varepsilon_{k'}} \right]. \quad (16)$$

Note the “−” sign in the above expression. Its importance will become apparent later when we discuss the renormalization flow for the coupling constants.

3.3 Renormalization of J_\pm

Finally, let us consider the scattering processes that contribute to the renormalization of the transverse (J_\pm) Kondo interaction. These are the processes that involve both the longitudinal and transverse terms, in which the electron is scattered from an initial state \uparrow to a final state \downarrow with a coherent flip of the impurity spin. Repeating the arguments similar to those used to derive Eqs. (13) and (14), one finds that the Feynman diagram in Fig. 2a results in the following contribution to the T matrix:

$$\Delta T_{\downarrow\uparrow}^{(a)}(\omega) = \frac{J_+ (-J_z) |\rho \delta\Lambda| S_z S^+ c_{\mathbf{k}'\downarrow}^\dagger c_{\mathbf{k}\uparrow}}{\omega - \Lambda + \varepsilon_k} + \frac{J_+ J_z |\rho \delta\Lambda| S^+ S_z c_{\mathbf{k}'\downarrow}^\dagger c_{\mathbf{k}\uparrow}}{\omega - \Lambda + \varepsilon_k}. \quad (17)$$

The signs of the two terms are opposite because in the first expression, the spin-flip happens first, so that J_z term scatters two spin- \downarrow states, resulting in the overall minus sign: $-J_z S_z c_{\mathbf{k}'\downarrow}^\dagger c_{\mathbf{k}\downarrow}$, whereas in the second term the order of spin-flips is the opposite so that $J_z S_z c_{\mathbf{q}\uparrow}^\dagger c_{\mathbf{k}\uparrow}$ contributes with the positive sign. Using the identities $S_z S^+ = S^+ / 2$ and $S^+ S_z = -S^+ / 2$, we see that both terms contributes equally to the S^+ term:

$$\Delta T_{\downarrow\uparrow}^{(a)} = -\frac{J_+ J_z |\rho \delta\Lambda| S^+ c_{\mathbf{k}'\downarrow}^\dagger c_{\mathbf{k}\uparrow}}{\omega - \Lambda + \varepsilon_k}. \quad (18)$$

Similarly, the diagram in Fig. 2b contributes in two ways

$$\Delta T_{\downarrow\uparrow}^{(b)}(\omega) = \frac{J_+ J_z |\rho \delta\Lambda| S_z S^+ c_{\mathbf{k}\uparrow}^\dagger c_{\mathbf{k}'\downarrow}}{\omega - \Lambda - \varepsilon_{k'}} + \frac{J_+ (-J_z) |\rho \delta\Lambda| S^+ S_z c_{\mathbf{k}\uparrow}^\dagger c_{\mathbf{k}'\downarrow}}{\omega - \Lambda - \varepsilon_{k'}}. \quad (19)$$

Using the spin identities, we conclude that this results in

$$\Delta T_{\downarrow\uparrow}^{(b)}(\omega) = \frac{J_+ J_z |\rho \delta\Lambda| S^+ c_{\mathbf{k}\uparrow}^\dagger c_{\mathbf{k}'\downarrow}}{\omega - \Lambda - \varepsilon_{k'}} = -\frac{J_+ J_z |\rho \delta\Lambda| S^+ c_{\mathbf{k}'\downarrow}^\dagger c_{\mathbf{k}\uparrow}}{\omega - \Lambda - \varepsilon_{k'}}, \quad (20)$$

where the last equality is obtained by changing the order of the creation/annihilation operators (incurring a minus sign). Collecting together the contributions from Eq. (18) and (20), we find that J_+ is renormalized according to

$$\delta J_+ = -J_+ J_z \rho |\delta\Lambda| \left[\frac{1}{\omega - \Lambda + \varepsilon_k} + \frac{1}{\omega - \Lambda - \varepsilon_{k'}} \right]. \quad (21)$$

A similar result can be obtained for the renormalization of the J_- term, by considering the scattering from spin \downarrow into spin \uparrow state:

$$\delta J_- = -J_- J_z \rho |\delta\Lambda| \left[\frac{1}{\omega - \Lambda + \varepsilon_k} + \frac{1}{\omega - \Lambda - \varepsilon_{k'}} \right]. \quad (22)$$

3.4 Renormalization group flow

Summarizing our results so far, we conclude that elimination of the virtual scattering to the band edges results in a Hamiltonian that retains its Kondo form (neglecting the potential scattering terms such as Eq. 11). However, the coupling constants in Eq. (7) are renormalized as a result of integrating out the high-energy states: $J_\alpha \rightarrow J_\alpha + \delta J_\alpha$. It is said that J_α becomes a *running coupling constant*. By collecting the results obtained in Eqs. (16), (21), and (22) and assuming from now on that $J_+ = J_- = J_\pm$, we conclude that:

$$\delta J_z = -J_\pm^2 \rho |\delta\Lambda| \left[\frac{1}{\omega - \Lambda + \varepsilon_k} + \frac{1}{\omega - \Lambda - \varepsilon_{k'}} \right], \quad (23)$$

$$\delta J_\pm = -J_z J_\pm \rho |\delta\Lambda| \left[\frac{1}{\omega - \Lambda + \varepsilon_k} + \frac{1}{\omega - \Lambda - \varepsilon_{k'}} \right]. \quad (24)$$

The ω dependence underlines the fact that the renormalized interactions are retarded. However, for low-energy excitations relative to the conduction electron bandwidth or the cutoff Λ , the frequency dependence of the interactions can be neglected in the denominator. Similarly, since one is typically interested in the scattering of conduction electrons near the Fermi surface (on energy scales of the order of $k_B T$), the energies $\varepsilon_{k'}$ and ε_k can also be neglected compared to Λ . The resulting renormalization of the coupling constants can then be recast in terms of two coupled differential equations:

$$\frac{dJ_z}{d \ln \Lambda} = -2\rho J_\pm^2 \quad (25)$$

$$\frac{dJ_\pm}{d \ln \Lambda} = -2\rho J_z J_\pm. \quad (26)$$

Note that $\delta\Lambda$ is negative, and therefore $d(\ln \Lambda) = -|d\Lambda|/\Lambda$ in the above equations.

This logarithmic dependence of the coupling strength on the ultra-violet energy cutoff Λ is the essential idea behind the concept of the renormalization group. The above equations can be rewritten more conveniently by introducing the dimensionless coupling constants $g_\alpha \equiv J_\alpha \rho$ ($\alpha = z, \pm$) as follows:

$$\begin{aligned} \frac{dg_z}{d \ln \Lambda} &= -2g_\pm^2 + \mathcal{O}(g^3) \equiv \beta_z(g_\alpha) \\ \frac{dg_\pm}{d \ln \Lambda} &= -2g_z g_\pm + \mathcal{O}(g^3) \equiv \beta_\pm(g_\alpha). \end{aligned} \quad (27)$$

The right-hand side of these relations is called the *beta function*, using the established nomenclature. The isotropic case $J_z = J_{\pm}$ is particularly instructive, in which case we obtain

$$\frac{dg}{d \ln \Lambda} = -2g^2 + 2g^3 + \mathcal{O}(g^4), \quad (28)$$

where the second term on the right-hand side was obtained by considering the higher-order diagrams depicted in Figs. 2c and d.

Notice that to leading order in the coupling constant, the sign of the β -function in Eq. (28) is negative, meaning that as the energy cutoff Λ decreases, the corresponding coupling strength increases. For ferromagnetic interaction ($g < 0$), the coupling renormalizes to zero, $g \rightarrow 0$; however in the antiferromagnetic case, g remains positive and runs off to infinity as $\Lambda \rightarrow 0$. It is said that the theory tends towards strong coupling. This crucial difference between the ferromagnetic and the antiferromagnetic case is a quantum effect and should be understood as follows: If the impurity couples ferromagnetically to the conduction electrons (the so-called *s-d* model), the effect of such coupling becomes negligible at low temperatures. In other words, the impurity spin decouples from the conduction electron sea and becomes asymptotically free. In the case of antiferromagnetic (Kondo) interaction, on the other hand, the coupling is always relevant at low temperatures, no matter how weak the initial coupling strength. This means that a perturbative treatment of the Kondo model will break down at sufficiently low temperature of the order of the Kondo temperature T_K , and a non-perturbative approach is necessary to determine the low-temperature behavior. It was famously shown by Kenneth Wilson using numerical renormalization group (see Section 4.1) that the ground state of the Kondo model is a spin-singlet [1], forming due to the screening of the impurity spin by the conduction electrons. The antiferromagnetic Kondo model has a very interesting parallel with high-energy physics. In condensed matter physics, we are interested in the low-energy and low-temperature regime, i.e., the infra-red (IR) limit $\Lambda \rightarrow 0$, whereas high-energy particle physics concerns itself with the renormalization in the ultra-violet (UV) regime ($\Lambda \rightarrow \infty$). Bearing this distinction in mind, we note that the negative β -function is equivalent to the statement that the running coupling constants tends to zero as the energy cutoff Λ increases (provided $g > 0$ initially). This is similar to the celebrated phenomenon of the ‘‘asymptotic freedom’’ in quantum chromodynamics (QCD) where the interaction between quarks vanishes in the UV limit [14, 15]. For this reason, the Kondo impurity model is perhaps the simplest model that displays such behavior of the running coupling constant. Of course in condensed matter systems, the UV cutoff is not infinite as in QCD, but rather is fixed to be the conduction electron bandwidth D by the underlying crystalline lattice.

Returning to Eqs. (25-26), note that the following relation between J_z and J_{\pm} is valid:

$$\frac{dJ_z}{dJ_{\pm}} = \frac{J_{\pm}}{J_z}, \quad (29)$$

or, equivalently, $J_z dJ_z = J_{\pm} dJ_{\pm}$. Integrating both parts of this equation, we conclude that

$$J_z^2 - J_{\pm}^2 = \text{const.} \quad (30)$$

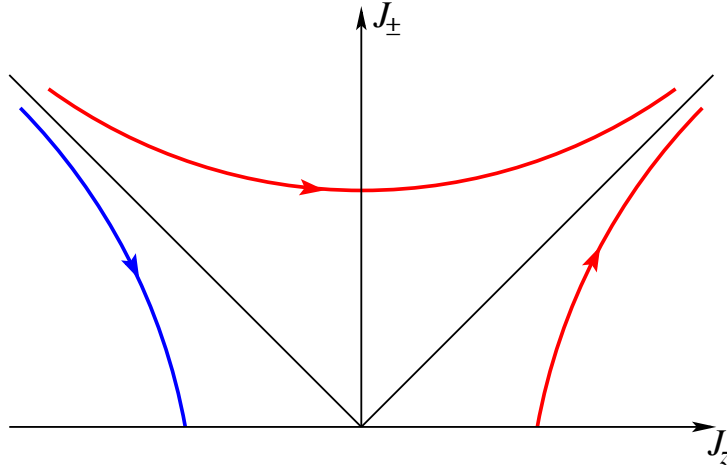


Fig. 3: Renormalization flow diagram of the anisotropic Kondo impurity model. On reducing the cutoff Λ , the coupling constants are scaled along the arrows. In the ferromagnetic region $J_z < 0$ and $|J_\pm| < |J_z|$, the system flows to weak coupling $J_\pm \rightarrow 0$ (blue arrow). In the rest of the parameter regime, the system flows towards the strong coupling regime $J_\alpha \rightarrow \infty$ (red arrows).

This is an example of a *scaling law* that holds at any point in the renormalization flow. Consequently, the renormalization group preserves the hyperbolic trajectories expressed by Eq. (30) and depicted in Fig. 3. It follows from Eq. (25) that the β -function for J_z is always negative, meaning that J_z always grows upon renormalization. For antiferromagnetic Kondo interactions, this indicates that the model flows towards the strong-coupling fixed point $(J_z, J_\pm \rightarrow \infty)$, as mentioned above for the isotropic case. The ferromagnetic case $J_z < 0$ requires extra care because the outcome depends on the ratio of $J_\pm/|J_z|$. The case $J_\pm < |J_z|$ corresponds to the constant being positive in the scaling relation (30) and since the β -function for J_\pm is positive, $J_\pm \rightarrow 0$ under the renormalization flow whereas $J_z < 0$ tends to a constant value, as indicated by the blue arrow in Fig. 3. In the other case $J_\pm > |J_z|$, J_\pm initially decreases, however it follows the hyperbolic curve, and at some point J_z changes sign to positive, at which point both coupling constants run off to infinity.

3.5 Kondo temperature and breakdown of the perturbative scheme

Using the above scaling results, we can estimate the temperature scale at which the perturbative approach to the antiferromagnetic Kondo problem breaks down. In what follows, we shall consider the isotropic case $J_z = J_\pm$, in which case the β -function is given by Eq. (28). Integrating both sides of Eq. (28), we obtain:

$$-\int_g^{g^*} \frac{dg}{g^2 - g^3} = 2 \ln \Lambda \Big|_D^{A^*} = -2 \ln \left(\frac{D}{\Lambda^*} \right) \quad (31)$$

The integral in the left-hand side can be evaluated to give

$$-\int \frac{dg}{g^2 - g^3} = \frac{1}{g} + \ln \left| 1 - \frac{1}{g} \right| \quad (32)$$

We expect perturbation theory to fail once the dimensionless running coupling constant becomes large $g^*(\Lambda^*) \gg 1$. Then, the terms of the order $1/g^*$ can be ignored in the left-hand side of Eq. (31) and Eq. (32), resulting in the expression for Λ^*

$$\Lambda^* \sim D \frac{\sqrt{g}}{\sqrt{1-g}} \exp\left(-\frac{1}{2g}\right), \quad (33)$$

which we can identify with the Kondo temperature $k_B T_K \sim \Lambda^*$. Taking into account the fact that the unrenormalized value of $g = \rho J \sim J/D$ is much smaller than 1, we can approximate $\sqrt{1-g} \approx 1$, resulting in the well known expression for the Kondo temperature

$$k_B T_K \sim \sqrt{J\rho} D \exp\left(-\frac{1}{2J\rho}\right). \quad (34)$$

This expression is non-analytic in J , confirming that it cannot be obtained via perturbation theory. Note that had we limited ourselves to the second-order diagrams in J only (Fig. 2a,b), the β -function in Eq. (28) would contain only the $-2g^2$ term, and the corresponding expression for the Kondo temperature would have a slightly different form: $k_B T_K^{(0)} \sim D \exp(-1/2J\rho)$, which only differs by an algebraic prefactor from Eq. (34).

One might worry that higher-order terms in the diagrammatic expansion used to obtain the β -function could generate new terms that are not present in the original Kondo Hamiltonian. However, such terms would behave as a power-law of $(1/\Lambda)^n$, rather than $\ln \Lambda$, and so tend to zero rather than diverge as the cutoff $\Lambda \rightarrow \infty$ (or equivalently, the conduction electron bandwidth $D \rightarrow \infty$). Such higher-order terms are *irrelevant* in the RG sense as they do not affect the low-temperature properties of the Kondo problem.

4 Low-temperature properties of the Kondo model

4.1 Wilson's numerical renormalization

The above scaling argument can be used down to energy scales larger than the Kondo temperature. Beyond that point, the running coupling constant diverges and the theory predictions cannot be trusted. An important breakthrough in this very difficult problem was achieved by Wilson [1], who transformed the model into a form appropriate for computer modeling and used a numerical renormalization algorithm to deduce the properties of the system. Below, we will explain briefly Wilson's line of reasoning. In a spherically symmetric system such as the single-impurity Kondo model, arbitrary real-space interactions $V(\mathbf{r} - \mathbf{R})$ can be expanded in spherical harmonics centered around the impurity site \mathbf{R} . Assuming the Kondo interaction to be a δ -function $\delta(\mathbf{r} - \mathbf{R})$, only the s -wave harmonic contributes, allowing one to describe the system as effectively one-dimensional, depending on the radial distance $|\mathbf{r} - \mathbf{R}|$ from the impurity site. Wilson further assumed the conduction electron dispersion to be linear $\varepsilon_k = k$ (here the Fermi velocity was set to 1 in the appropriate units with $-1 \leq k \leq 1$) and replaced it with a spectrum of discrete levels $\varepsilon_n = \Lambda^{-n}$ equally distributed on the logarithmic scale (here we use

Wilson's original notation, Λ should not be confused with the UV cutoff of the previous section). Then, the Hamiltonian of this discrete-level system can be written as a one-dimensional tight-binding chain with the 0-th site corresponding to the impurity position:

$$\mathcal{H}_N = \Lambda^{(N-1)/2} \left\{ \sum_{n=0}^{N-1} \Lambda^{-\frac{n}{2}} (c_n^\dagger c_{n+1} + c_{n+1}^\dagger c_n) - \tilde{J} c_0^\dagger \boldsymbol{\sigma} c_0 \cdot \mathbf{S} \right\}, \quad (35)$$

with the original Hamiltonian obtained after rescaling and taking the limit of an infinitely long chain: $\hat{H} = \lim_{N \rightarrow \infty} \Lambda^{-(N-1)/2} \mathcal{H}_N$.

The prefactor $\Lambda^{(N-1)/2}$ in front of the Hamiltonian is necessary to keep the scale of low-energy excitations constant. Note also that the hopping matrix element is proportional to $\Lambda^{-n/2}$ and decays quickly as a function of the distance from the impurity site.

4.2 Ground state of the Kondo model

The renormalized Kondo interaction $\tilde{J} \cdot \Lambda^{(N-1)/2}$ becomes large as the number of sites N increases, corresponding physically to the formation of a spin-singlet state on the impurity site. Wilson showed by careful numerical simulations that this is indeed the ground state of the Kondo model. Wilson also calculated the ratio of the uniform magnetic susceptibility and the specific heat coefficient (now known as the Wilson ratio) to be

$$W \equiv \lim_{T \rightarrow 0} \frac{T\chi/\chi_0}{C/\gamma_0} = 2. \quad (36)$$

This result is significant because of the conventional Fermi liquid result, where one has

$$\frac{C_{\text{FL}}}{T} \equiv \gamma_0 = \frac{\pi^2}{3} k_B^2 \rho, \quad \chi_{\text{FL}} \equiv \chi_0 = \frac{g^2 \mu_B^2}{4} \rho, \quad (37)$$

resulting in the Wilson ratio $W_{\text{FL}} = 1$ (as before, ρ is the density of states at the Fermi level). In the Kondo impurity case, the Wilson ratio is doubled. The classic work by Nozières [2] explains this as follows: The low-energy excitations of the Kondo model can be understood in the framework of the Fermi liquid theory. However in contrast to the one-body problem (where Wilson's ratio is 1), the interaction between the impurity and an electron with antiparallel spins contributes to the antisymmetric Fermi liquid parameter ϕ^a , which, as Nozières showed, leads to an additional contribution to the Wilson ratio. In the Kondo model, where this interaction becomes infinitely strong in the low-temperature limit, this extra contribution results in the Wilson ratio being 2. This is in line with the more general case of the Anderson Hamiltonian, where the Wilson ratio increases from 1 to 2 with increasing interaction U between antiparallel spins [16].

The Kondo model turns out to be exactly solvable via the Bethe ansatz, as shown independently by N. Andrei [3] and P. Wiegmann [4]. The exact solution fully confirmed Wilson's earlier conclusion that the ground state of the Kondo model is the spin singlet and corroborated Nozières' Fermi liquid theory.

5 Multichannel Kondo problem

Having described the behavior of the spin $1/2$ Kondo impurity model above, it is natural to ask: What happens in the case of impurity spin S larger than $1/2$? This problem was first addressed by Nozières and Blandin in 1980 [17], who formulated what we now refer to as the multichannel Kondo impurity model:

$$H = \sum_{\mathbf{k}, \sigma, \mu} \varepsilon_{\mathbf{k}} c_{\mathbf{k}\sigma\mu}^\dagger c_{\mathbf{k}\sigma\mu} + J \sum_{\mu=1}^K \mathbf{S} \cdot \boldsymbol{\sigma}_\mu, \quad (38)$$

where $\boldsymbol{\sigma}_\mu = \sum_{\mathbf{k}} c_{\mathbf{k}\alpha\mu}^\dagger \boldsymbol{\sigma}_{\alpha\beta} c_{\mathbf{k}\beta\mu}$ denotes the conduction electron spin in one of K orbital channels labeled by index μ . We shall only focus on the antiferromagnetic coupling J since the ferromagnetic case flows to weak coupling at low energies, as discussed earlier in Section 3.

5.1 Phenomenology and scaling

The multichannel model turns out to harbor rich physics, and depending on the number of conduction electron channels relative to the impurity spin size S , three different scenarios can be realized [17] (for a review, see also Ref. [18]):

- If $K = 2S$, the number of channels is exactly sufficient to fully compensate the impurity spin and the ground state is a spin singlet. This case, referred to as *perfect screening*, gives rise to the usual Fermi liquid behavior similar to the single-channel Kondo model discussed earlier in Section 4.
- If $K < 2S$, the impurity spin is not fully compensated since there are not enough conduction electron degrees of freedom. The dressed impurity remains magnetic with spin $S' = S - K/2$, resulting in the *underscreened* Kondo model.
- If $K > 2S$, the impurity spin is *overscreened*, resulting in the critical non-Fermi-liquid physics characterized by power-law or logarithmic behavior of thermodynamic quantities.

As the perfectly screened case needs little explanation, we will focus here on the latter two scenarios.

(1) Underscreened case $K < 2S$

Consider the spin \mathbf{S} maximally polarized along the z axis, $|S_z = S\rangle$. Because of the antiferromagnetic coupling to K conduction electron channels (each with spin $1/2$), part of the impurity spin will be screened as the energy cutoff Λ becomes lower than the Kondo temperature. The remaining spin $S' = S - K/2$ will be pointing along the z axis as shown in Fig. 4a. This resulting spin can still interact with the conduction electrons because the latter can perform virtual hops onto the impurity site from neighboring sites with characteristic strength $|J'| \sim \Lambda^2/J$ obtained in second-order perturbation theory (here the running cutoff $\Lambda \ll J$ under the RG

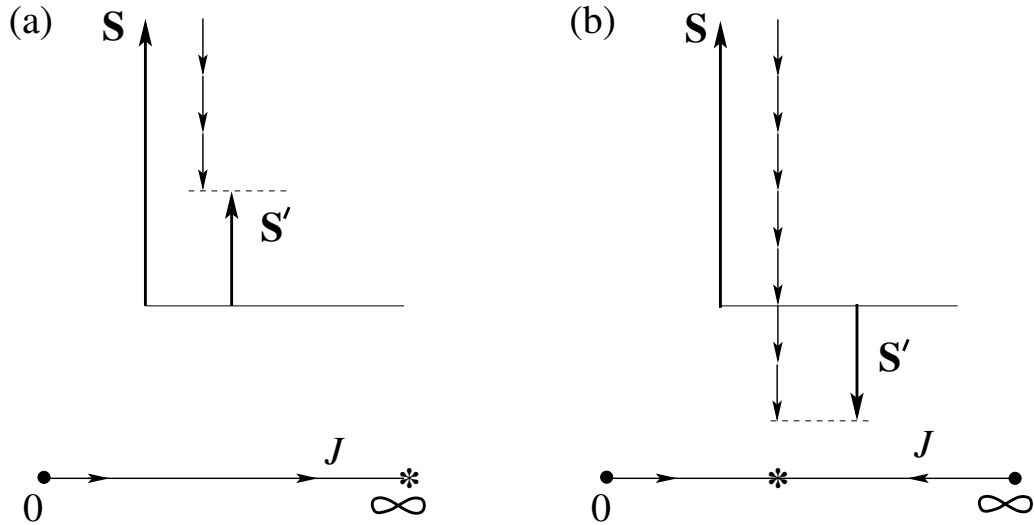


Fig. 4: Schematic depiction of the strong-coupling ground state of the impurity spin S and K conduction electron spins, together with the scaling trajectory for the running coupling constant J when (a) $K < 2S$, (b) $K > 2S$. A fixed point under the RG flow is denoted by asterisk (*).

process). The crucial point is that this coupling J' is *ferromagnetic*. Indeed, a nearby electron with \downarrow spin cannot jump onto the central site because all available orbital channels are already occupied by spin- \downarrow electrons as shown in Fig. 4a. Therefore, down spins do not interact with the unscreened impurity spin. By contrast, spin-up electrons can lower their energy in second-order perturbation theory by interacting with the unscreened spin S' that is also pointing up. Therefore, the residual coupling is indeed ferromagnetic and, as we know from Section 3, scales to weak-coupling under the RG flow, $J' \rightarrow 0$. Therefore, the $J \rightarrow \infty$ fixed point remains stable, as illustrated in the flow diagram in Fig. 4a.

(2) Overscreened case $K > 2S$

As in the previous case, the idea is to consider a two-stage process as the energy cutoff is reduced: First the Kondo singlet with the impurity spin forms, resulting from the strong coupling $J(\Lambda) \rightarrow \infty$. That leaves a residual interaction J' of the partially screened spin with the conduction sea. For a spin S along the z -axis, the conduction electron spins will “pile up” at the impurity site at sufficiently low energy Λ , generating an effective spin $S' = K/2 - S$ that is pointing down, opposite to the initial direction S_z (see Fig. 4b). Similar to the previous case, spin-down electrons do not participate in the virtual hopping onto the impurity site because all the spin-down states are already occupied (Pauli principle). Just as before, spin-up electrons can reduce their energy in second-order perturbation theory, generating an interaction $|J'| \sim \Lambda^2/J$ with the remaining impurity spin. The difference is that now S'_z is pointing *down*, so that the coupling J' to the conduction electrons is *antiferromagnetic*. However, we know that such an antiferromagnetic Kondo interaction scales to strong coupling as the cutoff is reduced, meaning that at sufficiently low Λ , the coupling $J'(\Lambda)$ is going to “blow up.” This is problematic because

our perturbative argument for $J' \sim \Lambda^2/J$ hinges on the fact that J' is small, otherwise perturbation theory does not converge. We conclude that the above two-stage RG process is untenable, meaning that the strong-coupling fixed point $J(\Lambda) \rightarrow \infty$ we assumed is actually unstable. The logical conclusion is that instead $J(\Lambda)$ should get renormalized to some finite value, leading to an *intermediate-coupling fixed point* denoted by the asterisk in Figure 4b.

Formally, one can see the appearance of the intermediate-coupling fixed point as follows. Consider the scaling equation obtained by summing the diagrams in Figures 2a-d. It has the form similar to Eq. (28) we derived in Section 3:

$$\frac{d(J\rho)}{d \ln \Lambda} = -2(J\rho)^2 + 2K(J\rho)^3 + \mathcal{O}(J\rho)^4, \quad (39)$$

except that the prefactor in the last term is now $2K$ instead of 2. This is because the closed loop in the diagrams in Fig. 2c and 2d contributes an additional factor of K due to the summation over the internal channel index $\mu = 1 \dots K$. Notice now that the beta-function on the right-hand side can be made to vanish at a *fixed point*

$$\rho J^* = \frac{1}{K}, \quad (40)$$

provided $J > 0$ (antiferromagnetic). When $K = 1$ as in the single-channel Kondo model, the result is meaningless because the expansion for the β -function in Eq. (39) does not converge. On the other hand for K large, the expansion becomes meaningful because every additional vertex yields a factor $J^* = 1/K$ and every additional loop yields a factor $K(J^*)^2 = 1/K$. Therefore, the expansion at the fixed point

$$\frac{d(\rho J^*)}{d \ln \Lambda} = -2\frac{1}{K^2} + 2K\frac{1}{K^3} + \frac{c}{K^4} + \frac{d}{K^5} + \dots \quad (41)$$

is well defined, thus making plausible the existence of the intermediate-coupling fixed point J^* . This conclusion, originally reached by Nozières and Blandin [17], was later confirmed by the exact solution obtained by the Bethe ansatz [19, 20] and by conformal field theory [21]. Unlike the strong-coupling fixed point in the one-channel Kondo model whose low-energy properties are described by Fermi-liquid theory [2], the intermediate-coupling case is characterized by its non-Fermi-liquid behavior. For instance, the exact solution of the multi-channel problem [19, 20] shows that the magnetic susceptibility and the specific heat both vary as

$$\chi \sim \frac{C}{T} \propto T^{\frac{4}{K+2}-1}, \quad K > 2 \quad (42)$$

In the particular case of $K = 2$, the power-law is replaced by a logarithmic temperature dependence:

$$\frac{C}{T} \sim \chi \propto \ln \left(\frac{T}{T_K} \right). \quad (43)$$

Of particular historical and practical importance is the (overscreened) two-channel Kondo problem for spin $S = 1/2$, which we shall analyze in more detail below.

5.2 Two-channel Kondo problem

The peculiarity of the intermediate-coupling fixed point predicted by Nozières and Blandin [17] is that at low temperatures, the running coupling constant flows to a fixed point with a finite value of J^* , regardless of how strong or weak the initial (bare) coupling is. This is remarkable because unlike the single channel model, nothing cuts off this scaling process and the impurity spin can never be screened. This means that there is no special energy scale analogous to the Kondo temperature in the single-channel model, and on approaching the fixed point, the system looks the same on all length scales. This inherent scale-invariance is the hallmark of a critical point, and like at any critical point, the correlation length ξ (the length at which the impurity spin affects the conduction electrons) diverges. It was shown by Affleck and Ludwig [21, 22] that this critical point is in fact described by a conformal field theory. Because of the criticality, various quantities are expected to scale as power-laws (or logarithmically, which can be viewed as a power-law with exponent zero). Indeed, as already mentioned, the intermediate coupling fixed point in the two-channel Kondo model is characterized by a logarithmic behavior of the magnetic susceptibility and the specific heat. The analysis by Ludwig and Affleck [22] further predicts the resistivity of the non-Fermi-liquid form:

$$\rho \sim \rho_0 + A\sqrt{T}. \quad (44)$$

A critical point generally requires fine-tuning, in other words, it may be destabilized by a relevant perturbation in the space of the model parameters. The two-channel Kondo model provides an illustrative example in that it is very sensitive to external perturbations. Below, we first consider the behavior under the application of the magnetic field that couples to the impurity spin, and then the effect of the channel anisotropy.

(a) Effect of the applied magnetic field

Because the impurity spin is never completely screened at the intermediate-coupling fixed point, the multichannel model displays a residual ground-state entropy. For the case of impurity spin $S = 1/2$, the residual entropy per impurity was calculated by the Bethe ansatz [19, 24]:

$$S(0) = \ln \left[2 \cos \left(\frac{\pi}{K+2} \right) \right]. \quad (45)$$

In the case of the two-channel model, the residual entropy $\frac{1}{2} \ln 2$ per impurity remains. However, application of an external magnetic field that couples to the impurity spin has a dramatic effect: It introduces a new energy scale $T_s \approx T_K (H/T_K)^{1+2/K}$ ($T_s \approx H^2/T_K$ in the two-channel case) that interrupts the scaling and below which the crossover to the screened, Fermi liquid behavior occurs. As a result, the residual entropy is removed in the $T \rightarrow 0$ limit. This is shown in Figure 5a, which displays the entropy as a function of temperature for several applied magnetic field strengths (reproduced from the numerical solution in Ref. [23]). This removal of the residual entropy has a spectacular signature in the temperature dependence of the specific heat. Above the crossover scale $T > T_s$, it behaves as a logarithm according to Eq. (43), but below this scale,

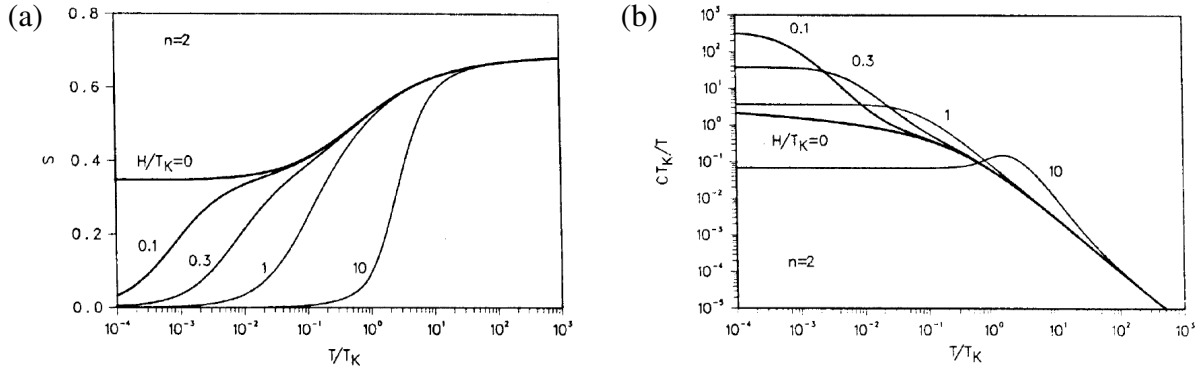


Fig. 5: Results for the two-channel Kondo model in an applied spin (magnetic) field: (a) entropy and (b) specific heat coefficient as function of temperature. The residual ground state entropy is released by the application of the field, while the specific heat develops a Schottky-like anomaly at the crossover scale T_s . (Reproduced from Ref. [23].)

the loss of the residual entropy manifests itself in a Schottky-like anomaly in the specific heat, shown in Fig. 5b. Notice that the value at the peak maximum can greatly exceed the $H = 0$ value of the specific heat, leading to a striking effect as a magnetic field is applied. A similar phenomenon occurs in the heavy fermion compound $Y_{1-x}U_xPd_3$, and it was suggested [25–27] that the multichannel Kondo model may provide an explanation, although of course one must remember that this is a dense Kondo lattice rather than an isolated impurity.

(b) Effect of the channel anisotropy

Unless there is a symmetry argument that requires the two orbital channels to couple to the impurity spin with identical strength, one might consider lifting this degeneracy by assigning two Kondo couplings $J_+ \neq J_-$:

$$H = \sum_{\mathbf{k}, \sigma} \sum_{\mu=\pm} \varepsilon_{\mathbf{k}} c_{\mathbf{k}\sigma\mu}^\dagger c_{\mathbf{k}\sigma\mu} + J_+ \mathbf{S} \cdot \boldsymbol{\sigma}_+ + J_- \mathbf{S} \cdot \boldsymbol{\sigma}_-. \quad (46)$$

Sometimes this is referred to as applying a “channel field” in that it splits the channels by an amount $\Delta J = J_+ - J_-$ similarly to the Zeeman splitting in the case of the “spin field.” It was argued that a real magnetic field can have this effect in the context of a quadrupolar Kondo effect [27]. Like in the case of the spin splitting described above, the channel anisotropy introduces a new crossover scale $T_{ch} \sim (\Delta J)^2/T_K$ that also cuts off the renormalization flow. However in this case, the consequences are much more dramatic: It was shown by Nozières and Blandin [17] that the more strongly coupled channel will tend towards the strong-coupling fixed point (as in the regular Kondo screening), whereas the weakly coupled channel will tend towards the zero-coupling fixed point. The resulting RG flow of the running coupling constants $J_\pm(\Lambda)$ is shown schematically in Fig. 6. The intermediate-coupling fixed point (marked by the black circle) is only stable along the $J_+ = J_-$ line but unstable for any small ΔJ . In particular, the fixed point is unstable along the separatrix shown with the dashed line in Fig. 6. The flow trajectories approach this separatrix on either side of the $J_+ = J_-$ line, depending on the sign of the bare ΔJ .

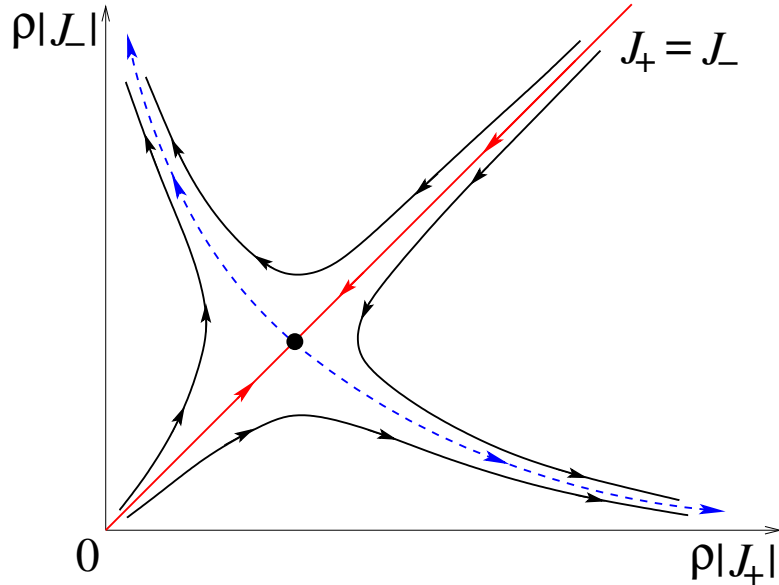


Fig. 6: Renormalization group flow of the anisotropic two-channel Kondo model for impurity spin $S = 1/2$ in the phase space of coupling constants. The flow to the intermediate coupling fixed point (filled circle) is stable only along the red line $J_+ = J_-$. The dashed blue line indicates the separatrix.

In conclusion, to observe the critical behavior of the two-channel spin-1/2 Kondo model and the associated non-Fermi liquid behavior, a perfect channel symmetry is required. In practice, this may be achieved if, for instance, the crystal point-group symmetry protects the system against the channel anisotropy. A conclusive experimental evidence of the non-Fermi-liquid behavior associated with the two-channel Kondo model is still lacking. This is partly due to the fact that the most promising candidates are in the dense Kondo lattice (rather than isolated impurity) limit. Nevertheless, the overscreened multichannel Kondo model displays rich physics and historically has played a very important role in the development of various theoretical tools used to study strongly correlated electron systems.

6 Kondo model in the presence of Hund's coupling

In the previous section, we have introduced the multi-channel Kondo impurity model. In particular, we stated that in the perfectly screened case $K = 2S$, the ground state of the problem is a spin-singlet, similar to the one-channel Kondo impurity model. A practical question arises, which we have not yet addressed: How does the Kondo temperature of such a multi-channel model depend on the size S of the impurity moment? Despite the deceiving simplicity, the answer to this question is not so simple and has not been fully appreciated until fairly recently, although the problem has a very interesting history dating back to the 1960s. One natural way of creating a large moment S on the impurity site is by Hund's coupling between $2S$ singly occupied orbitals, each with spin $s = 1/2$ (we shall use lower case s when referring to such a constituent impurity spin 1/2, not to be confused with the conduction electron spin σ). In this

section, we shall present the Poor Man's scaling theory of this problem and study its dependence on the size S of the impurity moment. The following discussion is based on the results of Ref. [28].

Let us consider K spin $s = 1/2$ impurity spins at a single site, ferromagnetically interacting via Hund's coupling J_H , each coupled to a conduction electron channel of bandwidth D via an antiferromagnetic interaction J :

$$H = \sum_{\mathbf{k}, \sigma, \mu} \varepsilon_{\mathbf{k}} c_{\mathbf{k}\sigma\mu}^\dagger c_{\mathbf{k}\sigma\mu} - J_H \left(\sum_{\mu=1}^K \mathbf{s}_\mu \right)^2 + J \sum_{\mu=1}^K \mathbf{s}_\mu \cdot \boldsymbol{\sigma}_\mu, \quad (47)$$

where $\varepsilon_{\mathbf{k}}$ is the conduction electron energy, $\mu = 1, \dots, K$ is the channel index and $\boldsymbol{\sigma}_\mu = \sum_{\mathbf{k}} c_{\mathbf{k}\alpha\mu}^\dagger \boldsymbol{\sigma}_{\alpha\beta} c_{\mathbf{k}\beta\mu}$ is the conduction electron spin density in channel μ at the origin. We implicitly assume that Hund's scale KJ_H is smaller than D .

The behavior of this model is well understood in the two extreme limits [17]: for $J_H = \infty$, the K spins lock together, forming a K -channel spin $S = K/2$ Kondo model studied in the previous section. The opposite limit $J_H = 0$ describes K replicas of the spin-1/2 Kondo model. Paradoxically, the leading exponential dependence of the Kondo temperature on the coupling constant $k_B T_K \sim D e^{-1/2J\rho}$ in these two limits is independent of the size of the spin. Naively, interpolating between these limits, one would conclude that the spin size does not enter into the Kondo temperature. However, it has been long known experimentally that this is not the case: the Kondo temperature of dilute d -metal impurities shows a striking dependence on the impurity spin, as shown in Fig. 7. The left panel is borrowed from the classic review paper by Daybell [29], based on the original experimental finding reported by Daybell and Steyert in 1968 [30]. What they noticed is that the Kondo temperature has a characteristic V-shape when plotted against the occupation of the d -electron level. For clarity, these data have been re-plotted as a function of the impurity spin in Fig. 7b, showing an impressive suppression of the Kondo temperature over five orders of magnitude when S is varied from $S = 1$ in Ti^{2+} and Ni^{2+} to $S = 5/2$ in Mn^{2+} .

Amazingly, this exponential dependence of the Kondo temperature on the impurity spin size had been predicted in 1967 by Schrieffer [31] before the experimental findings (in fact, Daybell and Steyert used Schrieffer's prediction to fit the data in Fig. 7a):

$$T_K^*(S) \approx D \exp\left(-\frac{2S}{2J\rho}\right) = T_K \left(\frac{T_K}{D}\right)^{2S-1}, \quad (48)$$

where $T_K \sim D e^{-1/2J\rho}$ is the leading exponential term in the Kondo temperature for spin 1/2 (cf. Eq. 34), and we have set $k_B = 1$ for convenience. Schrieffer obtained this result in the limit of infinitely strong Hund's coupling J_H , which we will explain later in this section.

Intriguingly, the experimental results and Schrieffer's early work from the 1960s were largely forgotten and have been re-discovered much more recently by the author and P. Coleman [28], who used the framework of Anderson's Poor Man's scaling to deduce the exponential suppression of the Kondo temperature with the impurity spin and generalized Schrieffer's analysis to finite J_H . This interesting phenomenon, referred to as the *Kondo resonance narrowing* due to Hund's coupling, is the main subject of this section.

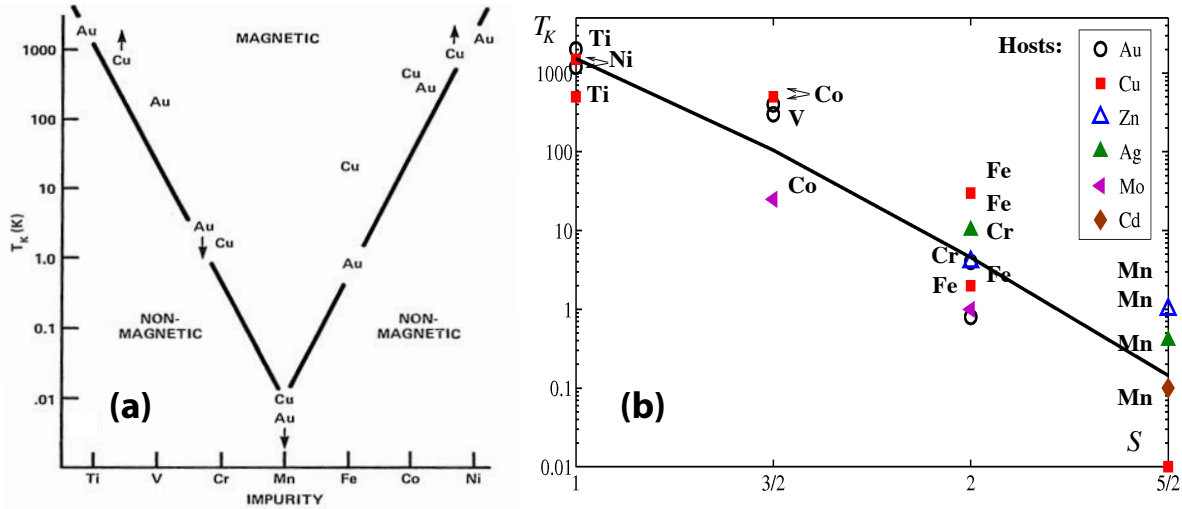


Fig. 7: Measured values of the Kondo temperature T_K^* in host alloys Au, Cu, Zn, Ag, Mo, and Cd containing transition metal impurities: (a) plotted vs. the d -level occupation of the impurity (Reproduced from Ref. [29]); (b) plotted vs. the nominal size S of the spin on the impurity site (Reproduced from Ref. [28]). Solid line is the fit to Eq. (63) with $\Lambda_0 \equiv J_H S$.

6.1 Poor man's scaling with Hund's coupling

We employ the Poor Man's scaling approach [13] described in detail in Section 3, in which the leading renormalization group (RG) flows are followed as the conduction electron degrees of freedom are systematically integrated out from the Hilbert space. The present exposition follows closely that in Ref. [28], where the scaling theory of the Kondo problem in the presence of Hund's coupling was first derived.

In the course of renormalization, one must be careful to consider the cutoff scale Λ relative to the other scales in the problem, in particular Hund's coupling J_H . We thus break up the energy integration into two intervals: (I) $J_H S < \Lambda < D$ and (II) $T_K^* < \Lambda < J_H S$, where T_K^* is the renormalized Kondo temperature (to be determined) below which the problem runs off to strong coupling.

Regime I: $J_H S < \Lambda < D$. In this regime Hund's coupling has no effect to leading order on the renormalization of the Kondo coupling J . In other words, the impurity $s = 1/2$ spins are decoupled from each other at high energies/temperatures, as illustrated schematically in Fig. 9a. We then arrive at the same equation (28) for the β -function obtained earlier in Section 3:

$$\frac{d(J\rho)}{d \ln \Lambda} = -2(J\rho)^2 + 2(J\rho)^3. \quad (49)$$

The Hund's coupling itself also gets renormalized, and the contributions to the β function are captured by the Feynman diagrams in Fig. 8. We shall not go into the details of calculating these diagrams but will quote the final result:

$$\frac{d(J_H \rho)}{d \ln \Lambda} = 4(J\rho)^2 J_H \rho \quad (50)$$

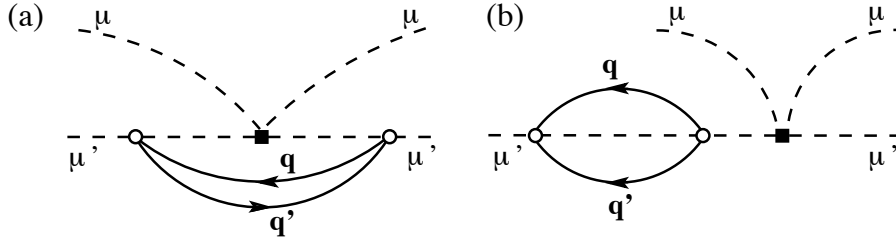


Fig. 8: The lowest-order Feynman diagrams in the RG flow of Hund's coupling. Solid lines denote the conduction electron propagators and dashed lines the impurity spins' (labeled by the channel number μ, μ'). A square vertex denotes Hund's coupling J_H , a circle the Kondo interaction J .

Thus the Hund's strength itself becomes a running coupling constant, whose value is renormalized down as the Kondo coupling $J\rho(\Lambda)$ grows:

$$\ln \left(\frac{\tilde{J}_H(\Lambda)}{J_H} \right) = -4 \int_{\Lambda}^D (\rho J(\Lambda))^2 d(\ln \Lambda). \quad (51)$$

This downward-renormalization of the Hund's coupling is, however, weak and to leading logarithmic order, we can approximate $J_H(\Lambda)$ to be constant.

Integrating both sides of Eq. (49) similarly to the procedure in Section 3.5, we find that as the cutoff Λ is reduced from the electron bandwidth D down to the Hund's scale $J_H S$, to leading logarithmic order we obtain a new renormalized Kondo coupling

$$\frac{1}{2J_I\rho} = \frac{1}{2J\rho} + \ln \Lambda \Big|_{\Lambda=D}^{J_H S}, \quad (52)$$

which grows upon renormalization as expected, $J_I > J$. Expressing the bare Kondo coupling in terms of the Kondo temperature $2J\rho = \ln^{-1}(D/T_K)$, we can rewrite the above expression as follows (we set $k_B = 1$ for convenience):

$$2\rho J_I = \ln^{-1} \left(\frac{J_H S}{T_K} \right). \quad (53)$$

Regime II: $T_K^* < \Lambda < J_H S$. Once Λ is reduced below $J_H S$, the individual local moments become locked into a spin $S = K/2$, as illustrated schematically in Fig. 9. This is the same effect as discussed by Jayaprakash *et al.* in Ref. [32] for the case of two impurities coupled by ferromagnetic RKKY interaction and as realized in the limit of $J_H \rightarrow \infty$ analyzed by Schrieffer in his 1967 paper [31].

The low-energy properties of the system in region II are described by a Kondo model of spin $K/2$ with K conduction electron channels:

$$H_{\text{eff}}^{\text{II}} = J^*(\Lambda) \sum_{\mu=1}^K \mathbf{S} \cdot \boldsymbol{\sigma}_{\mu}, \quad (54)$$

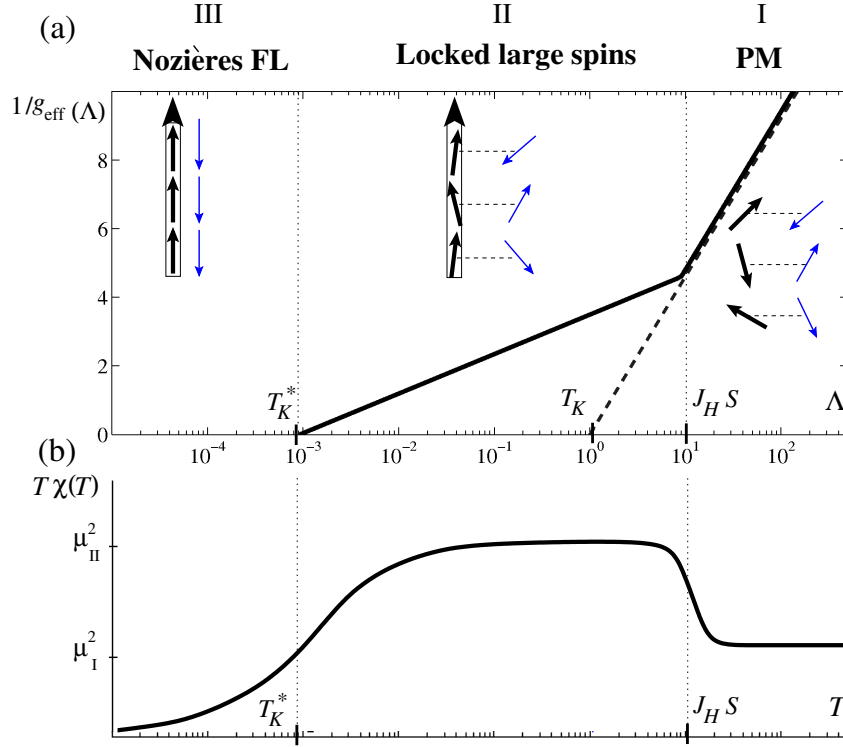


Fig. 9: (a) Schematic showing the behavior of the running coupling constant $g_{\text{eff}}(\Lambda) = J(\Lambda) \rho K_{\text{eff}}$ on a logarithmic scale, with K_{eff} the effective number of conduction electron channels per impurity spin ($K_{\text{eff}} = 1$ in region I and K in regions II and III). (b) Schematic showing effective moment $\mu_{\text{eff}}^2(T) = T \chi(T)$ in terms of the susceptibility $\chi(T)$ showing an enhancement in region II (see Eq. 68) and a loss of localized moments due to Kondo screening in region III.

however with the renormalized value of the Kondo coupling J^* . In order to obtain the value of J^* , we must project the original model onto the subspace of maximum spin S . By the Wigner-Eckart theorem, any vector operator acting in the basis of states $|S_z\rangle$ of spin $S = K/2$ is related by a constant prefactor to \mathbf{S} itself:

$$\langle SS_z | \mathbf{s}_\mu | SS_z \rangle = g_S \langle S_z | \mathbf{S} | S_z \rangle. \quad (55)$$

Summing both sides of the equation over the impurity index $\mu = 1, \dots, K$, one obtains

$$\langle SS_z | \sum_{\mu} \mathbf{s}_\mu | SS_z \rangle = g_S K S_z. \quad (56)$$

However, since $\sum_{\mu} \mathbf{s}_\mu = K \mathbf{s} \equiv \mathbf{S}$, one arrives at the conclusion that $g_S K = 1$, hence determining the value of the constant coefficient $g_S = 1/K$ in Eq. (55). Therefore, the Kondo interaction in the original model (47) can be cast in the form

$$J \sum_{\mu=1}^K \mathbf{s}_\mu \cdot \boldsymbol{\sigma}_\mu = J g_S \sum_{\mu=1}^K \mathbf{S} \cdot \boldsymbol{\sigma}_\mu. \quad (57)$$

Comparing this equation with Eq. (54) and substituting $g_S = 1/K$, we arrive at the following expression for the effective Kondo coupling:

$$J^* = \frac{J}{K} \equiv \frac{J}{2S}. \quad (58)$$

This equation captures the key effect of the crossover from region I to region II in Fig. 9. This result was first derived in the early work on the multi-channel Kondo problem by Schrieffer [31], where the limit of $J_H \rightarrow \infty$ was implicitly assumed, and also appears for the particular case of $K = 2$ in the study of the two-impurity Kondo problem by Jayaprakash *et al.* [32].

Having established the value J^* of the coupling constant, we now proceed with the Poor Man's renormalization of the effective model in Eq. (54). The scaling equation for $J^*(\Lambda)$ in region II involves calculating the same diagrams for the T matrix (see Fig. 2) as we have done earlier for the multichannel Kondo model in Eq. (39), with the result

$$\frac{d(J^*\rho)}{d \ln \Lambda} = -2(J^*\rho)^2 + 2K(J^*\rho)^3, \quad (59)$$

where the prefactor K in the last term appears due to the summation over the channel index $\mu = 1 \dots K$ inside the conduction electron bubble in the diagrams in Fig. 2c and 2d.

To one loop order, the β -function for $J^*(\Lambda)$ in region II is identical to that of region I, see Eq. (49). However, now the value of J^* is K times smaller according to Eq. (58). To avoid the discontinuous jump in the coupling constant at the crossover from region I to region II in Figure 9, it is more convenient to consider a dimensionless coupling constant

$$g_{\text{eff}} \equiv J^*(\Lambda) \rho K_{\text{eff}}, \quad (60)$$

which is designed to be smooth at the crossover from I to II by requiring that the effective number of channels $K_{\text{eff}} = 1$ and K in regions I and II, respectively. It follows from Eq. (59) that this continuous variable satisfies

$$\frac{d g_{\text{eff}}}{d \ln \Lambda} = -\frac{2}{K_{\text{eff}}} g_{\text{eff}}^2 + \frac{2}{K_{\text{eff}}} g_{\text{eff}}^3, \quad (61)$$

so the speed at which it scales to strong coupling becomes K times smaller in region II (see Fig. 9a). Solving this RG equation to leading order, and setting $g_{\text{eff}}(\Lambda = T_K^*) \sim 1$, we obtain $T_K^* \sim (J_H S) (D/J_H S)^K e^{-\frac{K}{2J\rho}}$ for the renormalized Kondo scale. Comparing this with the bare Kondo scale $T_K \sim D e^{-1/2J\rho}$ and denoting $J_H S = \Lambda_0$, we deduce

$$T_K^* \sim \Lambda_0 \left(\frac{T_K}{\Lambda_0} \right)^{2S} \equiv T_K \left(\frac{T_K}{\Lambda_0} \right)^{2S-1}, \quad (62)$$

showing that the effective Kondo temperature is exponentially suppressed by a factor of $(2S - 1)$ compared to its bare value for spin 1/2. When plotted on a logarithmic scale, the Kondo temperature is expected to scale linearly with the size of the impurity spin:

$$\ln T_K^*(S) = \ln \Lambda_0 - (2S) \ln \left(\frac{\Lambda_0}{T_K} \right), \quad (63)$$

which fits well the experimental data by Daybell and Steyert [30] for dilute d -electron impurities in Fig. 7.

Regime III: $A < T_K^*$. When the energy cutoff (or temperature) drops below the Kondo temperature in Eq. (62), the Poor Man's scaling predicts that the Kondo coupling runs off to infinity, as discussed in detail in Section 3. In this regime, the perturbative renormalization scheme employed above breaks down and alternative methods are necessary to establish the fate of the ground state.

In essence, Hund's coupling converts a one channel Kondo model (more precisely, K copies of the one-channel model) to a K -channel Kondo model but with a larger impurity spin $S = K/2$. As discussed in Section 5, the behavior of the perfectly screened multi-channel Kondo model is known from the seminal work of Nozières and Blandin [17] to be a Fermi liquid, with the conduction electrons screening the impurity spin. Of particular interest is the Wilson ratio defined in Eq. (36), which for the K -channel Kondo model was shown [17] to be

$$W = \frac{2(K+2)}{3}, \quad (64)$$

reducing to the value $W = 2$ in the one-channel case [2]. The above result holds in the limit of infinitely strong Hund's coupling. For a finite value of J_H , a crossover occurs between a 1-channel (region I) and a K -channel Kondo model (region II), as illustrated in Fig. 9a. While the Wilson ratio is difficult to determine in this case, we expect its value to depend on the ratio $\eta = U^*/J_H^*$, where U^* is the effective intra-channel interaction in the underlying Anderson model in the limit $T \rightarrow 0$, and J_H^* is the renormalized Hund's coupling (recall that Hund's coupling is a running coupling constant whose value is not constant, see Eq. (50)). We estimate [28] the Wilson ratio to be

$$W(\eta) = 2 \left(1 + \frac{K-1}{1+2(1+\eta)} \right), \quad (65)$$

which reproduces the result of Eq. (64) in the $\eta \rightarrow 0$ limit ($J_H \rightarrow \infty$).

6.2 Experimental ramifications of Hund's coupling

A. Effective moment crossover as a function of temperature

One of the observables sensitive to the Kondo narrowing is the effective spin on the impurity site, which we expect to change from spin 1/2 in regime I at high temperatures ($T > J_H S$) to effective spin $S = K/2$ at temperatures much lower than J_H . The effective impurity moment can be extracted from the Curie magnetic susceptibility, which we estimate to be:

Regime I: A spin-1/2 disordered paramagnet is characterized by a high temperature Curie magnetic susceptibility (g is the electron g-factor):

$$\chi_1(T) = \frac{K}{2} \left(\frac{1}{2} + 1 \right) \frac{(g\mu_B)^2}{3T}, \quad (66)$$

with effective moment $(\mu_{\text{eff}}^1)^2 = 3K/4$ in the conventional units of $(g\mu_B)^2$.

Regime II: The magnetic impurity susceptibility in region II can be calculated perturbatively for $T \gg T_K^*$ by keeping the leading logarithms $\ln(T/T_K)$ (see e.g. Ref. [7]):

$$\chi_{\text{imp}}^* = \frac{(g\mu_B)^2}{3T} S(S+1) \left(1 - \frac{1}{\ln\left(\frac{T}{T_K^*}\right)} + \mathcal{O}\left(\frac{1}{\ln^2\left(\frac{T}{T_K^*}\right)}\right) \right). \quad (67)$$

Substituting $S = K/2$, we see that the magnetic moment is enhanced at the crossover from region I to II as expected, with the ratio given by

$$\left(\mu_{\text{eff}}^{\text{II}}/\mu_{\text{eff}}^{\text{I}}\right)^2 = (K+2)/3 \quad (68)$$

Note that the above ratio is equal, up to the factor of 2, to the Wilson ratio in Eq. (64), which was obtained in the idealized $J_H \rightarrow \infty$ limit.

Regime III: Below the Kondo scale T_K^* , the Curie contribution to the susceptibility vanishes because the impurity moment becomes completely screened, as already mentioned above.

The temperature behavior of $T\chi(T)$, which is proportional to the effective moment squared, is plotted schematically across these three regimes in Fig. 9b. As described above, it shows an enhancement of the effective moment on the crossover from regime I to II and eventually vanishes due to Kondo screening as $T \rightarrow 0$ in regime III.

B. Suppression of the Kondo temperature

Next, we return to the behavior of the Kondo temperature, Eq. (62) which is the central result of this section. It follows from fitting the experimental data in Fig. 7 to our formula Eq. (63), that the bare value of T_K is of the order of 3000 K ($k_B T_K \sim 0.3$ eV), too large to observe for dilute spin-1/2 impurities. However, the Kondo temperature is drastically suppressed for larger values of spin, for instance $T_K^* \approx 20$ K for Fe impurities ($S = 2$) in Cu [30], from which we extract the ratio $T_K/\Lambda_0 \equiv T_K/(J_H S) \sim 0.2$ consistent with the known value of Hund's coupling $J_H \sim 0.7$ eV in d -electron metals. In the case of Mn impurities ($S = 5/2$), the suppression is so dramatic that T_K^* is unobservably low, probably in the milli-Kelvin range. In this regard, it is fitting to quote a visionary remark from Schrieffer's 1967 paper [31] (written before the experimental discovery!):

“Since $\exp(-1/J^\rho)$ varies so rapidly with $J^*\rho$, is it not possible that for modest variations of this parameter, T_K could sweep from millidegrees to beyond the melting point of metals?”*

C. Kondo resonance narrowing

The exponential suppression of the Kondo temperature as a function of impurity spin in the limit of large Hund's coupling has an important consequence for the electron spectral function $A_{\mathbf{k}}(\omega) \equiv -\frac{1}{\pi} \text{Im}(G_{\mathbf{k}}^R(\omega))$, where G^R is the retarded propagator. Detailed analysis of the spectral function is beyond the subject of this lecture, but for our purposes, it is sufficient for the reader to know that at low temperatures $T \ll T_K$, the formation of the spin singlet in the Kondo

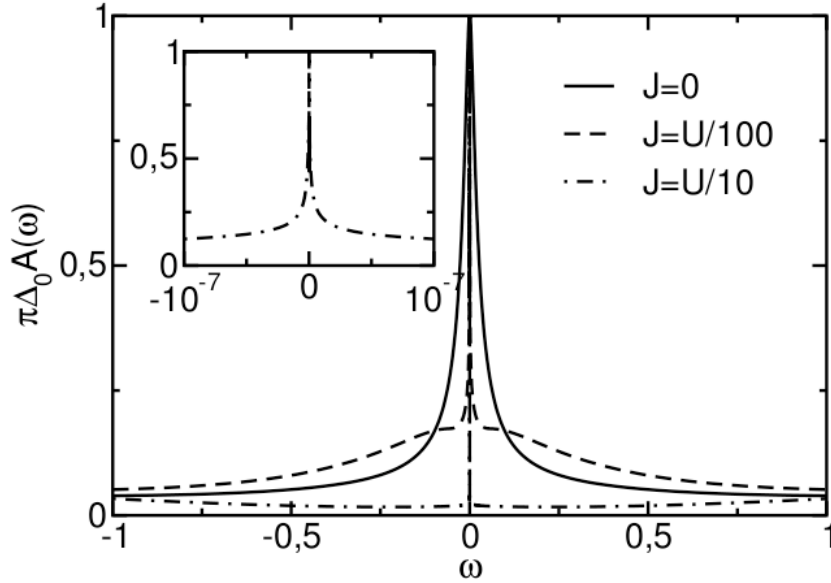


Fig. 10: Local electron density of states calculated with NRG at $T = 0$ for a particle-hole symmetric two-orbital Anderson impurity model with varying strength of Hund's coupling J . The Coulomb parameter U and the hybridization Δ_0 were chosen such that the system is in the Kondo limit. The Kondo resonance width is dramatically reduced upon increasing J (see inset for $J = U/10$). (Reproduced from Ref. [33])

impurity model manifests itself in a sharp peak near zero energy, known as the Abrikosov-Suhl resonance. The width of this peak is known to be of the order of the Kondo temperature. Thus, the suppression of the Kondo temperature because of Hund's coupling on the impurity site should result in the commensurate narrowing of the Kondo resonance peak. Direct experimental measurement of the Kondo resonance is not an easy task, however resonance narrowing was noticed in numerical renormalization group study of the two-orbital Anderson model by Pruschke and Bulla [33], reproduced in Figure 10. A dramatic resonance narrowing, by a factor of 10^{-7} , occurs by introducing a large value of $J_H = U/10$, where U is the interaction strength in the Anderson impurity model. While not understood at the time, this numerical evidence is in perfect agreement with the Kondo resonance narrowing effect described above. More recently, a number of numerical studies have confirmed this effect (for a comprehensive review, see Ref. [34]).

In itinerant systems, such as the iron-based superconductors, Hund's coupling was also found to play an important role, enhancing the effect of electron correlations. In particular, the so-called coherence temperature T^* , as inferred from the broad "hump" in resistivity measurement, was predicted to decrease drastically as the Hund's coupling strength is increased in numerical calculations [35]. Of course in this case, the localized moments are periodically arranged (as described by the Hubbard or periodic Anderson model) rather than centered on isolated impurity sites. Nevertheless it is tempting to associate the coherence temperature T^* with the typical lattice Kondo scale T_K^* . The latter should be suppressed dramatically by the Hund's coupling, explaining qualitatively the behavior in the Hubbard model. For more details, we refer the reader to the review by Georges *et al.* [34].

Conclusions

In this Lecture, we have outlined the basic ideas of the renormalization group (RG) approach and shown how they apply, in the simplest form, to the Kondo impurity model. This simplified renormalization procedure, known as Poor Man's scaling, captures the salient features of the Kondo problem. In particular, we showed how logarithmic singularities arise and how they can be summed up to result in the RG equation for the running coupling constant $J(\Lambda)$ that is cutoff-dependent. The essential feature of the antiferromagnetic Kondo model is that the running coupling constant grows upon renormalization and the resulting theory tends to strong coupling. At that point, the perturbative expansion in J is no longer reliable and an alternative approach is called for. We now know that the ground state of the Kondo model turns out to be a Fermi liquid, with impurity spin completely compensated (screened) by the conduction electrons. This important result was first obtained by Wilson's numerical renormalization and Nozières' phenomenological theory, and later confirmed by the exact solution of the Kondo model.

Having established these results for the simplest Kondo model, we then considered somewhat more complicated models that arise in realistic systems: the multichannel Kondo problem and the effect of Hund's coupling at the impurity site. Naturally, given the time and space constraints, we have only scratched the surface in analyzing these more complex cases. The reader is referred to the original papers and review articles for more detailed information, as well as to an excellent textbook by Yamada [6] and an encyclopedic monograph by Hewson [7]. Nevertheless, we hope to have given the reader a sense of what the Kondo problem is and how one goes about solving it within the scaling approach. The appeal of the Kondo problem also lies in the fact that, in addition to its rich underlying physics, the ideas we have developed in the course of this lecture are quite general and apply to many other branches of physics, both in condensed matter and in high-energy physics. Personally, I find this very satisfying and perhaps this accounts for the reason why, in addition to its historical significance, the Kondo model is such a fascinating topic. Finally, let me add that the lattice generalization of this model, the so-called Kondo lattice model, is still unsolved and remains an active subject of research to date, with important consequences for heavy fermion materials (see lecture by Piers Coleman in this School).

Acknowledgements

The author is grateful for the hospitality of the Institute of Solid State Physics, University of Tokyo, Japan where he held a Visiting Professor appointment in summer 2015 during which this Lecture was conceived.

References

- [1] K.G. Wilson, Rev. Mod. Phys. **47**, 793 (1975)
- [2] P. Nozières, J. Low Temp. Phys. **17**, 31 (1974)
- [3] N. Andrei, Phys. Rev. Lett. **45**, 379 (1980)
- [4] P.B. Wiegmann, Sov. Phys. JETP Lett. **3**, 392 (1980)
- [5] P. W. Anderson, J. Phys. C **3**, 2436 (1970)
- [6] K. Yamada: *Electron Correlations in Metals* (Cambridge University Press, 2004)
- [7] A.C. Hewson: *The Kondo Problem to Heavy Fermions* (Cambridge Univ. Press, 1993)
- [8] W.J. de Haas and G.J. van den Berg, Physica **3**, 440 (1936)
- [9] J. Kondo, Prog. Theor. Phys. **32**, 37 (1964)
- [10] J. Kondo, Solid State Phys. **23**, 183 (1969)
- [11] A.A. Abrikosov, Physics **2**, 5 (1965)
- [12] P.W. Anderson and G. Yuval, Phys. Rev. Lett. **23**, 89 (1969)
- [13] P.W. Anderson and G. Yuval, Phys. Rev. **131**, 1522 (1970)
- [14] D. Gross and F. Wilczek, Phys. Rev. Lett. **30**, 1343 (1973)
- [15] H. Politzer, Phys. Rev. Lett. **30**, 1346 (1973)
- [16] K. Yamada, Prog. Theor. Phys. **53**, 970 (1975)
- [17] P. Nozières and A. Blandin, J. Phys. (Paris) **41**, 193 (1980)
- [18] P. Schlottmann and P.D. Sacramento, Adv. Phys. **42**, 641 (1993)
- [19] N. Andrei and C. Destri, Phys. Rev. Lett. **52**, 364 (1984)
- [20] A.M. Tsvelik and P.B. Wiegmann, Z. Phys. B: Condens. Matter **54**, 201 (1984)
- [21] I. Affleck and A.W.W. Ludwig, Nucl. Phys. B **352**, 849 (1991)
- [22] A.W.W. Ludwig and I. Affleck, Phys. Rev. Lett. **67**, 3160 (1991)
- [23] P.D. Sacramento and P. Schlottmann, Phys. Rev. B **43**, 13294 (1991)
- [24] A.M. Tsvelik, J. Phys. C **18**, 159 (1985)

-
- [25] C.L. Seaman, M.B. Maple, B.W. Lee, S. Ghamaty, M.S. Torikachvilli, J.-S. Kang, L.Z. Liu, J.W. Allen, and D.L. Cox, *Phys. Rev. Lett.* **67**, 2882 (1991)
- [26] C.L. Seaman, M.B. Maple, B.W. Lee, S. Ghamaty, M.S. Torikachvilli, J.-S. Kang, L.Z. Liu, J.W. Allen, and D.L. Cox, *J. Alloys Compounds* **181**, 327 (1992)
- [27] D. Cox and A. Zawadowski, *Adv. in Phys.* **47**, 599 (1998)
- [28] A.H. Nevidomskyy and P. Coleman, *Phys. Rev. Lett.* **103**, 147205 (2009)
- [29] M. Daybell: In G. Rado and H. Suhl (eds.) *Magnetism* (Academic Press, New York, 1973), Vol. 5, pp. 122–147
- [30] M.D. Daybell and W.A. Steyert, *Rev. Mod. Phys.* **40**, 380 (1968)
- [31] J.R. Schrieffer, *J. Appl. Phys.* **38**, 1143 (1967)
- [32] C. Jayaprakash, H.R. Krishna-murthy, and J.W. Wilkins, *Phys. Rev. Lett.* **47**, 737 (1981)
- [33] T. Pruschke and R. Bulla, *Eur. Phys. J. B* **44**, 217 (2005)
- [34] A. Georges, L. de' Medici, and J. Mravlje, *Ann. Rev. Condens. Matter Phys.* **4**, 137 (2013)
- [35] K. Haule and G. Kotliar, *New J. Phys.* **11**, 025021 (2009)